The Meteoritical Society

Meteoritics & Planetary Science 42, Nr 7/8, 1121–1134 (2007)
Abstract available online at http://meteoritics.org

3-D elemental and isotopic composition of presolar silicon carbides

Torsten HENKEL[1†*], Thomas STEPHAN[1], Elmar K. JESSBERGER[1], Peter HOPPE[2], Roger STREBEL[2, 3], Sachiko AMARI[4], and Roy S. LEWIS[5]

[1]Institut für Planetologie/ICEM, Wilhelm-Klemm-Strasse 10, 48149 Münster, Germany
[2]Max-Planck-Institut für Chemie, Postfach 3060, 55020 Mainz, Germany
[3]Physikalisches Institut, Universität Bern, Sidlerstrasse 5, 3012 Bern, Switzerland
[4]Laboratory for Space Sciences and Physics Department, Washington University, Saint Louis, Missouri 63130, USA
[5]Enrico Fermi Institute, University of Chicago, Chicago, Illinois 60637, USA
†Present address: School of Earth, Atmospheric, and Environmental Sciences, The University of Manchester, Oxford Road, Manchester, M13 9PL, UK
*Corresponding author. E-mail address: torsten.henkel@manchester.ac.uk

(Received 18 October 2006; revision accepted 13 April 2007)

Abstract–Thirteen presolar silicon carbide grains—three of supernova (SN) origin and ten of asymptotic giant branch (AGB) star origin—were examined with time-of-flight–secondary ion mass spectrometry (TOF-SIMS). The grains had been extracted from two different meteorites—Murchison and Tieschitz—using different acid residue methods. At high lateral resolution of ~300 nm, isotopic and elemental heterogeneities within the micrometer-sized grains were detected. The trace elemental abundances, when displayed in two-element correlation plots, of Li, Mg, K, and Ca show a clear distinction between the two different meteoritic sources. The different concentrations might be attributed to differences of the host meteorites and/or of extraction methods whereas the stellar source seems to be less decisive. In one SN grain with ^{26}Mg-enrichment from extinct ^{26}Al, the acid treatment, as part of the grain separation procedure, affected the Mg/Al ratio in the outer rim and therefore the inferred initial ^{26}Al/^{27}Al ratio. A second SN grain exhibits a lateral heterogeneity in ^{26}Al/^{27}Al, which either is due to residual Al-rich contamination on the grain surface or to the condensation chemistry in the SN ejecta.

INTRODUCTION

Presolar grains condensed in the environments of stars from gas ejected during late stages of their evolution. The grains therefore reflect the specific elemental and isotopic compositions of their stellar sources. They contribute to the interstellar medium from which new stars and planets like our solar system form and survived in primitive solar system material from which they can be extracted. Except for diamonds, analyses of individual grains are possible since their first isolation from meteorites in 1987 (Lewis et al. 1987; Bernatowicz et al. 1987). They reveal large isotopic variations of up to several orders of magnitude that distinguish them from solar material and trace individual grains back to their specific sources. Diamond and recently discovered silicates are most abundant among presolar grains, with concentrations of more than 100 ppm in primitive meteorites and interplanetary dust particles (Anders and Zinner 1993; Nguyen and Zinner 2004; Mostefaoui and Hoppe 2004; Floss et al. 2006). The presolar SiC grains, typically making up a few ppm of the host meteorite, are separated into seven groups: types A, B, X, Y, Z, and mainstream grains and a small population of nova grains. Most of the SiC grains are attributed to 1–3 $M_\odot$ AGB stars with varying metallicity. Exceptions are the rare type X grains, which are assigned to supernovae (Amari et al. 1992; Hoppe et al. 2000). For recent reviews, see Hoppe and Zinner (2000), Nittler (2003), Zinner (2004), and Lodders and Amari (2005) and references therein.

Most grains have been extracted from the host meteorites using acid residue methods where the host meteorite is dissolved in a series of different acids (Amari et al. 1994). These treatments are quite harsh and only acid-resistant phases survive the process, biasing the variety of presolar grains for subsequent investigation. In addition, the acids may alter the grains during the extraction process.

Table 1. Sample overview showing name, type of presolar SiC, size, and the host meteorite for the all analyzed grains. Additional data is given for the Murchison grains which had been analyzed with the IMS3f before (n.d. = not determined).

Name	Type	Size (μm)	Host meteorite	$\delta(^{29}Si/^{28}Si)$	$\delta(^{30}Si/^{28}Si)$	$^{12}C/^{13}C$	$^{14}N/^{15}N$	$(^{26}Al/^{27}Al)_0$	Al/Si
KJG2-243-U	Mainstream	2.0	Murchison	47	36	5.8	4612	0.0035	0.092
KJG2-243-O	A + B	5.5 × 3.5	Murchison						
KJG2-333	A + B	2.7	Murchison	35	5	10.1	2955	0.0020	0.081
KJG2-415	Mainstream	1.9	Murchison	70	61	48.2	1348	0.0002	0.123
KJG2-422	X	3.3	Murchison	−376	−585	1135	18.1	0.2000	0.047
KJG2-422-SiC	Mainstream	3.7 × 1.9	Murchison	n.d.	n.d.	n.d.	n.d.	n.d.	n.d.
177-1	X	2.0	Tieschitz	n.d.	n.d.	n.d.	n.d.	n.d.	n.d.
480-3	X	1.5	Tieschitz	n.d.	n.d.	n.d.	n.d.	n.d.	n.d.
SiC 1	Mainstream	2.5	Tieschitz	n.d.	n.d.	n.d.	n.d.	n.d.	n.d.
SiC 2	Mainstream	2.2	Tieschitz	n.d.	n.d.	n.d.	n.d.	n.d.	n.d.
SiC 3	A + B	2.0	Tieschitz	n.d.	n.d.	n.d.	n.d.	n.d.	n.d.
SiC 4	Mainstream	2.3	Tieschitz	n.d.	n.d.	n.d.	n.d.	n.d.	n.d.
SiC 5	Mainstream	1.5	Tieschitz	n.d.	n.d.	n.d.	n.d.	n.d.	n.d.

Time-of-flight–secondary ion mass spectrometry (TOF-SIMS) allows comprehensive studies by recording complete secondary ion spectra for positive and negative secondary ions (Stephan 2001). Therefore, it allows elemental and isotopic analyses of many elements simultaneously with high lateral resolution, sufficient to analyze these grains on a submicrometer scale. Another great advantage is the low sample consumption of only a few nanometers during a single measurement, making it possible to do depth profiling at high resolution. The depth resolution will be slightly compromised due to the naturally rough surface of the grains, which leads to different angles of incidence and therefore different sputter rates (see, e.g., Rost et al. 1999). The small sample consumption of typically less than 1% for a 2 micrometer-sized grain is very small compared to the sample consumption of most double-focusing SIMS (DF-SIMS) instruments like the Cameca IMS3f or similar which will sputter ~50% of the grain for a similar analysis and have been the main instruments in presolar grain analysis until the recent introduction of the Cameca NanoSIMS.

Previous TOF-SIMS studies with high lateral resolution (Stephan et al. 1996, 1997) showed lateral heterogeneities of Al within presolar SiC grains from the Murchison meteorite and also changes with depth which might be due to the destruction of Al during the chemical processing. Further studies (Henkel et al. 2000, 2002) confirmed interior structures not only in the Al abundance but for other elemental and isotopic ratios. Silicon- and Ca-isotopic heterogeneities were reported by Besmehn and Hoppe (2003) for type X grains. Elemental heterogeneities in the form of TiC and AlN sub grains as well as oxide rims have been observed in TEM studies of SiC grains (e.g., Stroud and Bernatowicz 2005; Hynes et al. 2006). The aim of this study is to take advantage of the TOF-SIMS capabilities for spatially resolved analyses of presolar grains while recording whole mass spectra to find out more about elemental and isotopic heterogeneities within presolar SiC.

SAMPLES

Presolar silicon carbide grains from the Murchison CM chondrite (6 grains) and the Tieschitz H/L-chondrite (7 grains) were analyzed (Table 1). The Murchison grains stem from the size-separated fraction KJG (Amari et al. 1994) with sizes between 2.1 and 4.5 μm and have been analyzed with DF-SIMS before using the IMS3f ion microprobe at Washington University in Saint Louis. One of these grains (KJG2-422) showed the typical signs of a SN grain (type X) in the DF-SIMS measurement; the others were of type A + B (KJG2-243-O and -333) or mainstream grains (KJG2-243-U, -415, and -422-SiC). No DF-SIMS data exists for KJG2-422-SiC. KJG2-243-O and -U were formerly classified and analyzed by DF-SIMS as one grain, but turned out to consist of two separate grains lying just next to each other.

The Tieschitz grains were prepared in a less destructive way than the Murchison ones in order to search for presolar oxide grains that normally would be destroyed in the harsh acid treatment (Strebel 1998). The main difference compared to the Murchison extraction process is that the last step using H_2SO_4 to destroy spinel and chromite was omitted. The grains have been analyzed with isotopic imaging in the IMS3f ion microprobe at the University of Bern to find grains of type X for other studies (Strebel 1998). The sample consumption for these measurements is estimated to be less than 100 nm. During isotopic imaging, images of ^{28}Si and ^{30}Si distribution are taken to find grains enriched in ^{28}Si, a characteristic signature of SN grains. Among the grains for this study were two of type X (177-1 and 480-3). All grains were in the size range of 1–7 μm, and the non-SN grains were named SiC-1 to SiC-5 (all mainstream grains, except for SiC-3, which is of type A + B).

EXPERIMENTAL METHODS

A TOF-SIMS instrument from ION-TOF, Münster, Germany was used for this study. It is equipped with a 25 kV

Ga primary ion gun, which delivers a DC current of ~2 nA of primary ions into a spot size with a diameter of ~300 nm. The secondary ions are detected using a reflectron type time-of-flight analyzer. Further details are given in the literature (Stephan 2001).

To achieve the necessary mass resolution ($m/\Delta m_{FWHM}$ of ~3500 at ^{28}Si) for resolving hydrides from atomic peaks while keeping the lateral resolution at ~300 nm, the instrument was used in the so-called chopper mode. The primary ion beam is chopped into short packets of ~1.5 ns using a 40 MHz beam blanking signal resulting in ~10 primary ions per shot. Using the normal pulsing unit, one to several of these pulses can then be selected and the rest are blanked (Stephan 2001).

The measurements were done in a scanning mode with 128 × 128 pixels for each scan and 32 primary ion shots per pixel, with fields of view of usually 10 × 10 μm^2 and 15 × 15 μm^2 for one bigger grain. A single measurement lasted about 400 to 500 scans (8–10 h) resulting in a primary ion dose of up to 3–4 × 10^9 primary ions. The primary ion dose density with a field of view of 10 × 10 μm^2 was therefore around 3–4 × 10^{15} primary ions/cm^2. Secondary ion (SI) distribution images can be extracted from the recorded raw data by selecting individual peaks in the mass spectrum.

Due to temperature changes and/or electronic instabilities, the position of the ion beam can shift from scan to scan during such long measurements with a total shift of up to a few micrometers. Therefore, a shift correction was applied before single scan images were overlaid for the total image. The Si image was then used to mark the grain area and regenerate the total grain spectrum from raw data taking the sample shift into account. Where appropriate, further analyses have been performed on subregions of grains. Quantification for element abundances is done using sensitivity factors relative to Si derived from well-characterized, homogeneous glass standards (Stephan 2001) because homogeneous SiC standards with known trace element contents were not available.

Even at the achieved high mass resolution, hydrides and oxides are often not completely separated from elemental peaks. Therefore, the isotope ratios were determined with a peak deconvolution method. The peak shape of the main isotope is fitted to that of the minor isotope so that the isotope ratio is given by the scaling factor (Stephan 2001). Due to mass fractionation during the sputter process, an external correction of measured isotope ratios is necessary. Thus, special care was taken to determine the reproducibility and accuracy of isotopic measurements. Eight glass standards (MPI-DING) (Jochum et al. 2000) and one silicon carbide standard (NIST SRM 112b) of known composition with terrestrial isotope ratios were analyzed and the mass fractionations were determined. The results are shown in Table 2, giving the average instrumental mass fractionation for each isotope ratio and the standard deviation as a measure of the accuracy. There is no significant difference between the different materials of the used standards, making it possible to use mass fractionations from the silicates if they couldn't be determined from the SiC-standard.

The accuracy for most isotope ratios is in the range of a few percent because of the small duty cycle time of ~10^{-5}, which results in relatively low counting statistics and therefore high statistical errors compared to other methods like DF-SIMS. With primary ion doses in the range of 10^{10} ions and ionization yields of one secondary ion per 100 primary ions, one can expect approximately 10^8 secondary ions. Minor elements with abundances of roughly 100 ppm are detected with count numbers in the range of 10^4. With an isotope ratio of 100, the count number for the minor isotope will be in the range of 10^2. Therefore, statistical errors for isotope analyses with TOF-SIMS are typically in the 10% range for minor elements but only a few percent for major elements. The majority of presolar SiC grains has C-isotopic anomalies of several 10% and N-isotopic anomalies of more than a factor of 2, which can thus be recognized and measured with sufficient precision by TOF-SIMS. Counting statistics are limiting the measurable C or N isotope ratios to below several hundred depending on the total number of counts in each measurement because peak deconvolution is not possible any more if the minor isotope peak becomes too small. Other elements like Si have isotopic anomalies typically in the percent range and are thus hard to measure with sufficient precision by TOF-SIMS. However, the subgroup of the supernova X grains has Si-isotopic anomalies of several 10% and in this case also Si-isotopic measurements can be done with sufficient precision.

RESULTS

The elemental abundances have been determined for Li, Mg, Al, K, Ca, Sc, Ti, V, and Cr relative to Si in atomic ratios and are summarized in Tables 3 and 4 together with the determined isotope ratios. Because of the very low abundance of some of these elements, not all could be determined in all analyzed grains. Other elements could not be quantified because their abundance has been below the detection limit or mass interferences made a reliable quantification impossible. Additionally, there are no suitable standard reference materials available for N and F. A reliable quantification of C was not possible because C^+ ions in positive measurements can originate from hydrocarbon contamination which might not have been totally removed during sputter cleaning. In negative mode, the efficiency of C-ion formation is influenced by sputter deposition of Cs during the prior IMS3f measurements. Therefore reliable relative sensitivity factors for C were not available.

A comparison of the previously acquired IMS3f data for the Murchison grains with the TOF-SIMS results from this study shows a good agreement for most data. The Si isotope ratios agree within 2 sigma as do the C and N isotope ratios

Table 2. Instrumental mass fractionations from silicate and silicon carbide standard material measured by TOF-SIMS. Values are given as deviation from terrestrial standards in per mill (δ values). Errors are 1σ.

	MPI-DING standards			SRM 112b		
	Mass fractionation		Standard deviation	Mass fractionation		Standard deviation
$\delta(^{13}CN/^{12}CN)$	n.d.			–49	±	13
$\delta(C^{15}N/C^{14}N)$	n.d.			16	±	26
$\delta(^{25}Mg/^{24}Mg)$	1	±	11	–20	±	17
$\delta(^{26}Mg/^{24}Mg)$	–15	±	9	–36	±	17
$\delta(^{29}Si/^{28}Si)$	–34	±	29	–19	±	7
$\delta(^{30}Si/^{28}Si)$	–86	±	38	–68	±	31

for the grains for which we could determine these ratios. The agreement for the C and N isotope ratios also proves that there was no significant interference from $^{13}C_2$ or $^{11}B^{16}O$ on mass 26 and 27, respectively. There is a disagreement for some of the Al/Si abundance ratios and the initial, inferred $^{26}Al/^{27}Al$ ratios. The IMS3f measurements average over a bigger volume of the grain and sampled a different part of the grain. Heterogeneities, which have been observed in the in the Al distribution (see Fig. 4), could therefore be the explanation for the observed discrepancies.

Elemental Abundances

An overview of all elemental abundances is shown in Fig. 1. The abundances range from just above 10^{-6} (relative to Si) to almost 0.4 with relative big variations for all elements of at least two orders of magnitude. Mg shows a huge variation of over five orders of magnitudes whereas all other elements have variations of two to three orders of magnitude. Except for SN grain 480-3, which shows some very high Mg abundances of up to 25%, only Al is a major element, having abundances of per mills up to 40% in the SiC grains. The very high abundance of Mg in one of the grains (480-3) is possibly a subgrain dominated by Mg. An exact determination of the subgrain composition was impossible due to its small size (<300 nm) (Fig. 4). Aluminum was often found in subgrains like in grain 480-3, which explains the measured Al abundances of up to 40%. See Fig. 4 for a secondary ion image of this grain showing an Al-rich region, which is not correlated with the Mg subgrain just above it. In some grains Ca showed heterogeneous distributions, often correlated with Al. Further heterogeneous distributions have been found for Sc, V, and Ti, which are not correlated with the Mg and Al subgrains.

Although the number of grains analyzed in this study is small, there seems to be an overlap in abundance ranges for most elements measured with few exceptions. The Ti abundances for the Murchison grains show a difference between the SN grains and non-SN grains. This is also evident for the Ca abundances in Tieschitz and Murchison SN grains. By far the biggest differences are found for Mg, which shows a complete separation between Murchison and Tieschitz grains, which also results in the aforementioned wider range of Mg abundances.

Correlation coefficients for all element abundances have been calculated for further investigation and are listed in Table 5 for the Murchison grains and in Table 6 for the Tieschitz grains. Because of the low number of samples and because not all elemental abundances could be obtained, only a small number of data points exist for some of these correlations. This makes it necessary to determine the level of confidence for the found correlations using Student's t-test. The results for Murchison grains are very clear with levels of confidence above 99.8% for all correlation coefficients shown in bold numbers. For the Tieschitz data, the situation is less clear. We accepted all correlations with a level of confidence above 97.5%, but these correlations are often rather a trend than a strong correlation with correlation coefficients as low as 0.52. Some results for Sc seem to suggest a correlation, but we rejected these as the level of confidence was below 90%. The correlations for the Murchison grains between Al and Ca and also between Li, Mg, and K and between Sc, V, and Ti are quite strong. For the Tieschitz grains, the correlation between Sc, V, and Ti is as strong as for the Murchison grains, but the correlations between Li, Mg, Al, K, and Ca are rather a general trend.

Figure 2 shows these correlations as Li-Al, Mg-Al, K-Al, Ca-Al, Ti-Al, Li-K, Mg-K, Sc-Ti, and V-Ti diagrams. Especially, the Mg-Al, Ca-Al, Li-K, and Mg-K plots show a clear separation between the different meteorite sources, which was not observable when looking at single element abundance ranges only. Remarkably, the SN grains show similar elemental ratios as the non-SN grains. The plots for Li-Al and K-Al are less clear and the Ti-Al plot shows a separation between the different stellar sources with the SN grains being in the lower right part of the plot having high Al and low Ti contents. Similarly, the Sc-Ti and V-Ti plots are showing the same separation by the stellar source, with low Sc, Ti, and V contents for the SN grains and high abundances for the non-SN grains. A positive correlation between Ti and V was also seen by Kashiv et al. (2001, 2002), who determined Ti abundance ranges of 136–3551 ppm, which are compatible with these results. Some values in this study are up to a factor of 6 higher than the range given by Kashiv et al. (2001), but this is understandable because they measured bulk abundances whereas only very small volumes have been measured in this study, which for some analyses probably contain TiC subgrains but not for all.

Table 3. Elemental and isotopic ratios from TOF-SIMS analyses of three SiC SN grains. Grains 177-1 and 480-3 were measured three times and grain KJG2-422 twice. Grain 480-3 was additionally divided into three separate areas A, B, and C. Errors are 1σ. Mg abundances are calculated without ^{26}Mg which normally dominates the Mg signal for SN grains. $(^{26}Al/^{27}Al)_0$ ratios have been directly calculated from counts because the peak deconvolution, which was used to determine the $\delta(^{26}Mg/^{24}Mg)$ values, does not work for peaks which are too small. Elemental abundances given with "<" denote upper limits for these elements, where accurate values could not be determined because of possible interferences.

		177-1			480-3 1st			480-3 2nd
		1st	2nd	3rd	A	B	C	A
Li	$\times10^{-6}$	90 ± 20	140 ± 30	140 ± 20	460 ± 50	580 ± 60	580 ± 110	1050 ± 120
Mg	$\times10^{-6}$	940 ± 80	1800 ± 200	2400 ± 120	9500 ± 300	9500 ± 300	15,600 ± 800	4200 ± 300
Al	$\times10^{-3}$	47.8 ± 0.5	133 ± 2	96 ± 1	99.6 ± 1.2	168 ± 2	224 ± 3	193 ± 3
Si		≡ 1	≡ 1	≡ 1	≡ 1	≡ 1	≡ 1	≡ 1
K	$\times10^{-6}$	4940 ± 10	10,000 ± 200	8400 ± 100	11,200 ± 300	19,600 ± 200	29,200 ± 500	7900 ± 200
Ca	$\times10^{-6}$	8800 ± 200	13,200 ± 300	17,700 ± 300	13,600 ± 300	10,500 ± 200	10,000 ± 200	13,300 ± 500
Sc	$\times10^{-6}$	n.d.	n.d.	100 ± 30	n.d.	n.d.	n.d.	n.d.
Ti	$\times10^{-6}$	170 ± 50	700 ± 120	500 ± 90	350 ± 80	150 ± 60	240 ± 130	100 ± 80
V	$\times10^{-6}$	30 ± 20	30 ± 20	90 ± 30	10 ± 20	n.d.	n.d.	120 ± 60
$^{12}C/^{13}C$		87 ± 9	+ 82 ± 6	62 ± 5	n.d.	88 ± 8	n.d.	68 ± 16
$^{14}N/^{15}N$		35 ± 3	29 ± 2	31 ± 2	82 ± 11	98 ± 11	n.d.	n.d.
$\delta(^{25}Mg/^{24}Mg)$		60 ± 420	–60 ± 220	–180 ± 150	n.d.	n.d.	n.d.	n.d.
$\delta(^{26}Mg/^{24}Mg)$		238,000 ± 20,000	134,000 ± 11,000	118,000 ± 6400	n.d.	n.d.	n.d.	75,800 ± 6200
$(^{26}Al/^{27}Al)_0$		0.494 ± 0.009	0.231 ± 0.005	0.333 ± 0.006	0.17 ± 0.004	0.096 ± 0.002	0.074 ± 0.004	0.174 ± 0.006
$\delta(^{29}Si/^{28}Si)$		–410 ± 60	–280 ± 70	–470 ± 60	–240 ± 80	–290 ± 80	–170 ± 90	–320 ± 80
$\delta(^{30}Si/^{28}Si)$		–560 ± 60	–560 ± 60	–570 ± 60	–410 ± 60	–430 ± 60	–330 ± 90	–400 ± 80

		480-3 2nd		480-3 3rd			KJG2-422	
		B	C	A	B	C	1st	2nd
Li	$\times10^{-6}$	1460 ± 150	1100 ± 200	<80	380 ± 80	780 ± 130	350 ± 50	3100 ± 200
Mg	$\times10^{-6}$	44,000 ± 1000	270,000 ± 5000	1400 ± 200	53,800 ± 1400	83,000 ± 2000	50 ± 30	110 ± 80
Al	$\times10^{-3}$	309 ± 5	370 ± 6	192 ± 2	257 ± 3	371 ± 3	79.8 ± 1	97 ± 3
Si		≡ 1	≡ 1	≡ 1	≡ 1	≡ 1	≡ 1	≡ 1
K	$\times10^{-6}$	14,000 ± 400	21,400 ± 500	5000 ± 200	9300 ± 200	26,300 ± 400	2330 ± 80	17,800 ± 400
Ca	$\times10^{-6}$	12,200 ± 400	19,900 ± 800	13,000 ± 400	7100 ± 300	25,600 ± 700	550 ± 60	1000 ± 130
Sc	$\times10^{-6}$	n.d.	n.d.	n.d.	90 ± 60	30 ± 40	50 ± 30	300 ± 200
Ti	$\times10^{-6}$	420 ± 140	<300	440 ± 140	380 ± 140	190 ± 140	190 ± 60	400 ± 200
V	$\times10^{-6}$	n.d.	n.d.	90 ± 60	30 ± 40	n.d.	70 ± 40	60 ± 80
$^{12}C/^{13}C$		77 ± 14	83 ± 27	61 ± 24	n.d.	n.d.	n.d.	57 ± 6
$^{14}N/^{15}N$		n.d.	102 ± 44	98 ± 11	74 ± 10	59 ± 7	19 ± 3	25 ± 3
$\delta(^{25}Mg/^{24}Mg)$		150 ± 90	70 ± 50	n.d.	n.d.	n.d.	n.d.	n.d.
$\delta(^{26}Mg/^{24}Mg)$		5100 ± 230	450 ± 60	n.d.	n.d.	n.d.	n.d.	n.d.
$(^{26}Al/^{27}Al)_0$		0.075 ± 0.003	0.033 ± 0.005	0.171 ± 0.005	0.098 ± 0.004	0.055 ± 0.003	0.225 ± 0.005	0.255 ± 0.012
$\delta(^{29}Si/^{28}Si)$		–360 ± 80	–330 ± 120	–140 ± 100	–230 ± 80	–180 ± 90	–370 ± 60	–270 ± 110
$\delta(^{30}Si/^{28}Si)$		–500 ± 70	–340 ± 110	–400 ± 70	–330 ± 80	–520 ± 80	–520 ± 70	–470 ± 80

Table 4. Elemental and isotopic ratios for all non-SN grains. Most grains were measured twice except grains SiC 3 and 4 as well as KJG2-333 and -415. Errors are 1σ. Mg abundances are calculated without ^{26}Mg which normally dominates the Mg signal for SN grains.

Tieschitz		SiC 1		SiC 2		SiC 3	SiC 4	SiC 5	
		1st	2nd	1st	2nd			1st	2nd
Li	$\times10^{-6}$	170 ± 20	<24	<60	<30	<10	<100	<60	<70
Mg	$\times10^{-6}$	1980 ± 110	2300 ± 200	460 ± 40	300 ± 50	170 ± 50	1330 ± 110	810 ± 90	2940 ± 130
Al	$\times10^{-3}$	18.0 ± 0.4	45.3 ± 0.7	9.3 ± 0.2	8.1 ± 0.3	3.0 ± 0.2	17.6 ± 0.4	56.0 ± 0.9	91.1 ± 0.7
Si		≡ 1	≡ 1	≡ 1	≡ 1	≡ 1	≡ 1	≡ 1	≡ 1
K	$\times10^{-6}$	4970 ± 70	1060 ± 50	1320 ± 20	1410 ± 50	420 ± 30	4190 ± 90	2030 ± 60	2270 ± 50
Ca	$\times10^{-6}$	2240 ± 80	2400 ± 100	4340 ± 80	1240 ± 110	250 ± 40	12,600 ± 200	11,100 ± 200	10,200 ± 200
Sc	$\times10^{-6}$	n.d.	n.d.	n.d.	n.d.	200 ± 50	n.d.	n.d.	330 ± 60
Ti	$\times10^{-6}$	40 ± 20	n.d.	2200 ± 100	7500 ± 400	390 ± 80	1310 ± 140	390 ± 90	1460 ± 110
V	$\times10^{-6}$	15 ± 10	n.d.	40 ± 10	380 ± 60	n.d.	n.d.	n.d.	130 ± 30
^{12}C/^{13}C		56 ± 4	58 ± 6	57 ± 7	48 ± 9	8 ± 4	80 ± 20	62 ± 8	59 ± 5
^{14}N/^{15}N		n.d.	n.d.	111 ± 31	n.d.	62 ± 32	n.d.	n.d.	n.d.
δ(^{25}Mg/^{24}Mg)		−170 ± 200	n.d.	n.d.	100 ± 470	n.d.	n.d.	90 ± 380	n.d.
δ(^{26}Mg/^{24}Mg)		−150 ± 150	0 ± 200	n.d.	2700 ± 1400	n.d.	510 ± 300	430 ± 710	n.d.
(^{26}Al/^{27}Al)$_0$		n.d.	n.d.	n.d.	n.d.	n.d.	n.d.	0.0017 ± 0.0007	0.0014 ± 0.0005
δ(^{29}Si/^{28}Si)		57 ± 82	46 ± 74	36 ± 58	49 ± 66	180 ± 70	30 ± 71	190 ± 70	64 ± 67
δ(^{30}Si/^{28}Si)		160 ± 70	99 ± 73	37 ± 57	130 ± 70	20 ± 96	45 ± 73	64 ± 70	31 ± 66

Murchison		KJG2-243-U		KJG2-243-O		KJG2-333	KJG2-415	KJG2-422-SiC	
		1st	2nd	1st	2nd			1st	2nd
Li	$\times10^{-6}$	360 ± 40	470 ± 30	190 ± 20	70 ± 20	920 ± 90	110 ± 20	<15	200 ± 20
Mg	$\times10^{-6}$	60 ± 20	22 ± 11	24 ± 8	5 ± 2	30 ± 30	6 ± 5	18 ± 4	3 ± 4
Al	$\times10^{-3}$	401 ± 2	165.7 ± 0.8	109.6 ± 0.5	40.6 ± 0.2	152 ± 2	30.8 ± 0.3	63.7 ± 0.2	87.8 ± 0.5
Si		≡ 1	≡ 1	≡ 1	≡ 1	≡ 1	≡ 1	≡ 1	≡ 1
K	$\times10^{-6}$	3050 ± 60	2970 ± 50	1480 ± 20	864 ± 12	1390 ± 70	330 ± 10	124 ± 4	1080 ± 20
Ca	$\times10^{-6}$	7300 ± 200	2620 ± 80	1770 ± 40	410 ± 20	630 ± 70	190 ± 20	710 ± 20	580 ± 30
Sc	$\times10^{-6}$	640 ± 70	290 ± 40	1940 ± 70	470 ± 30	230 ± 70	230 ± 30	260 ± 40	290 ± 30
Ti	$\times10^{-6}$	3500 ± 200	9000 ± 300	45,600 ± 600	16,600 ± 200	8900 ± 500	11,700 ± 300	1340 ± 40	10,700 ± 200
V	$\times10^{-6}$	130 ± 30	730 ± 70	3110 ± 110	540 ± 30	820 ± 140	1110 ± 60	150 ± 10	560 ± 40
^{12}C/^{13}C		24 ± 4	30 ± 4	10 ± 4	11 ± 4	16 ± 4	55 ± 7	62 ± 5	64 ± 5
^{14}N/^{15}N		n.d.	n.d.	n.d.	n.d.	n.d.	n.d.	n.d.	n.d.
δ(^{25}Mg/^{24}Mg)		n.d.	n.d.	n.d.	n.d.	n.d.	n.d.	n.d.	n.d.
δ(^{26}Mg/^{24}Mg)		n.d.	n.d.	n.d.	n.d.	n.d.	n.d.	n.d.	n.d.
(^{26}Al/^{27}Al)$_0$		0.0015 ± 0.0002	0.0015 ± 0.0002	0.0146 ± 0.0005	0.0209 ± 0.0006	0.0027 ± 0.0005	0.0016 ± 0.0004	0.0017 ± 0.0001	0.0016 ± 0.0002
δ(^{29}Si/^{28}Si)		130 ± 73	240 ± 80	73 ± 60	−15 ± 57	−35 ± 90	53 ± 65	89 ± 54	220 ± 60
δ(^{30}Si/^{28}Si)		135 ± 67	75 ± 63	72 ± 58	58 ± 54	110 ± 90	17 ± 62	51 ± 54	92 ± 58

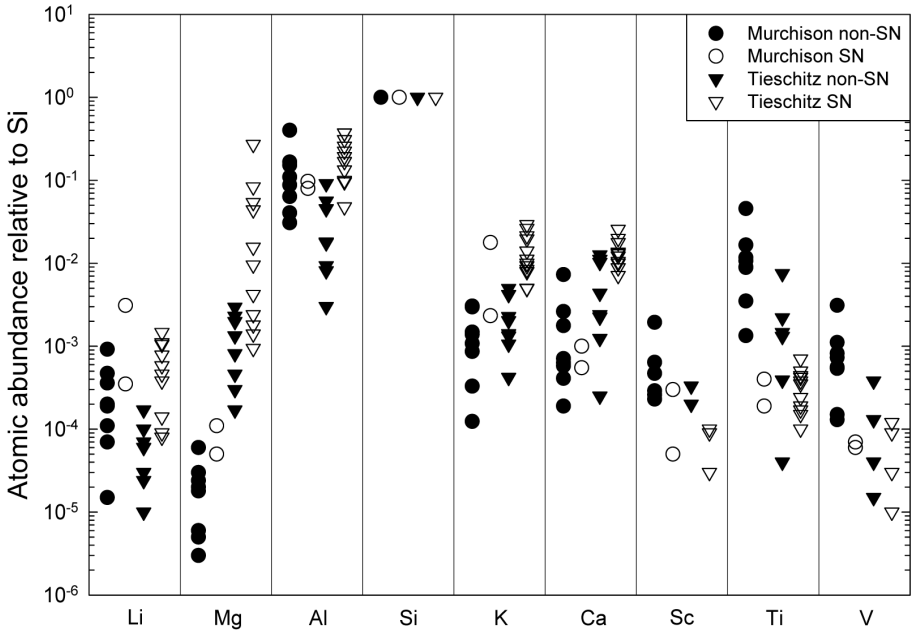

Fig. 1. Elemental abundances for the presolar SiC grains of this study. Elemental abundances are given relative to Si (i.e., Si ≡ 1). Most grains are represented by more than one data point because of multiple measurements, showing the variations found within the grains.

Depth Profiling of the Tieschitz Supernova Grains

Depth profiles have been taken of grains 177-1 and 480-3 from the Tieschitz meteorite down to a depth of around 40 nm. To achieve this depth, three measurements with intermediate heavy sputtering using an Ar-ion gun have been made. Before our TOF-SIMS studies, these grains have been analyzed with isotopic imaging of Si in the IMS3f ion microprobe to search for supernova grains. The original surface is therefore sputtered away and the surface from which the depth profile starts is already some ten nanometers into the grain. The results are shown in Figs. 3 and 5 and are discussed in detail in the following sections. The achieved depths for both measurements are calculated from the primary ion dose densities of our measurements assuming one sputtered particle for each primary ion. Because of different sputter rates for different angles of incidence and the three-dimensional shape of the sample, there will be variation in the sputter rate. The total variation should be small as this effect averages out while the grain is sputtered away resulting in a smoothed surface.

Grain 177-1

For the SN grain 177-1, the depth profiles for $^{26}Mg^+/^{28}Si^+$, Al/Si, and $^{12}C^{14}N^-/^{28}Si^-$ as well as the inferred, initial $^{26}Al/^{27}Al$, $^{14}N/^{15}N$, $^{28}Si/^{29}Si$, and $^{28}Si/^{30}Si$ isotope ratios are displayed in Fig. 3. The latter three isotope ratios clearly show the supernova signature of this material throughout the sputtered volume with no significant changes of their values. In contrast to the constant N- and Si-isotope ratios, the elemental ratios change significantly with depth. Because $^{26}Al/^{27}Al$ is calculated from $^{26}Mg^*/^{27}Al$ ($^{26}Mg^*$ is the excess ^{26}Mg stemming from the decay of radioactive ^{26}Al, which in this case dominates ^{26}Mg) this also holds for the $(^{26}Al/^{27}Al)_0$ ratio, which varies by more than a factor of two. This change mainly occurs because of the strong decrease in the ^{27}Al abundance toward the surface, whereas the $^{26}Mg^+/^{28}Si^+$ ratio only changes from the first to the second measurement by ~25%. The CN abundance changes similarly to the Al abundance as one would expect if Al and N exist as AlN within the SiC.

This grain does not show any lateral heterogeneity in any element for all measurements meaning that the changes are purely with depth. It also implies that there are no subgrains within this grain unless they are so small and numerous that the grain would appear homogeneous again, which is very unlikely. Therefore the changes in elemental abundances and isotope ratios cannot be attributed to the presence of subgrains.

Grain 480-3

Grain 480-3 showed lateral heterogeneities in several elements during all measurements and was therefore analyzed in more detail by dividing the grain into three subareas A, B, and C, as shown in Fig. 4.

The Si isotope ratios clearly identify this grain as of type X with enrichments in ^{28}Si, $\delta(^{29}Si/^{28}Si)$ between −140 and −370 per mil and $\delta(^{30}Si/^{28}Si)$ between −330 and −520 per mil. Additionally, it shows high excesses in ^{26}Mg, which, similar to grain 177-1, can be attributed to the decay of ^{26}Al. The inferred, initial $^{26}Al/^{27}Al$ ratios show a lateral heterogeneity for the three subregions A, B, and C (Fig. 5). Similar to grain

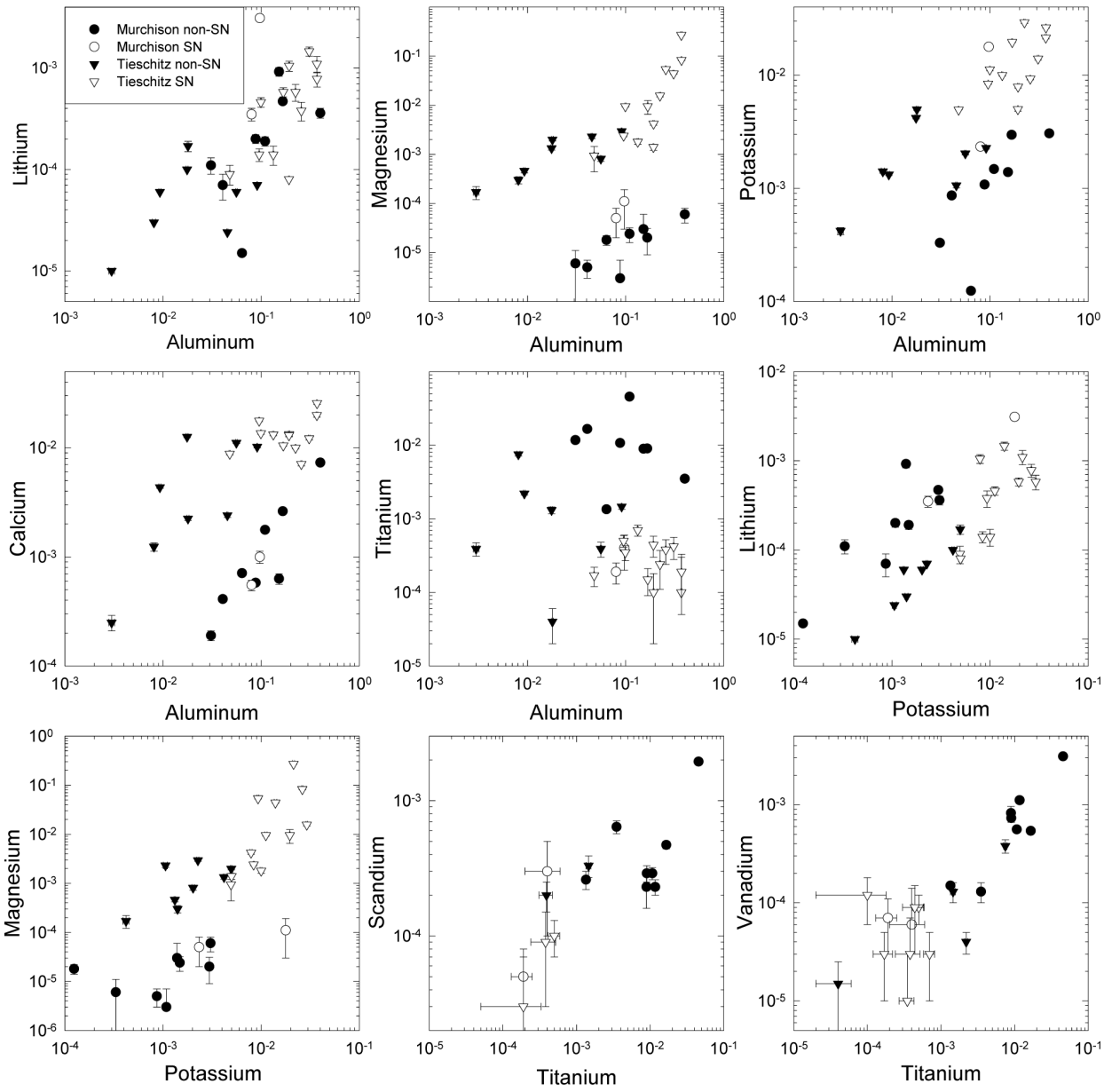

Fig. 2. Element versus element abundance diagrams (normalized to Si) for the presolar SiC grains of this study. Except for the Ti-Al, Sc-Ti, and V-Ti plots, which show a separation according to the stellar sources of the grains, all others show a more or less clear separation between the meteorite sources.

177-1, one can see changes in the $^{26}Mg^{+}/^{28}Si^{+}$ ratio and Al abundance while the grain is sputtered away, but in contrast to the other grain, resulting in almost constant $(^{26}Al/^{27}Al)_0$ ratios with depth in regions A and B, because ^{26}Mg (dominated by radiogenic Mg) and ^{27}Al change in the same way. The only significant change with depth occurs in area C, with variations as similarly observed for grain 177-1 (factor of two). A change by a factor of ~3 is seen laterally within the $(^{26}Al/^{27}Al)_0$-ratio from ~0.17 (area A) to ~0.09 (B) and, finally, to ~0.05 (C), left to right. The difference in $^{26}Al/^{27}Al$ between area C and area A is largely due to the higher ^{27}Al concentration in area C (Fig. 5).

DISCUSSION

Element Correlations

The elements correlating with the Al abundance for the Tieschitz grains are Li, Mg, K, and Ca, and the latter three are major elements of the host meteorite, which has been dissolved during the extraction process leading to possible contamination with meteoritic material. SiC itself is acid-resistant and should therefore not be dissolved or altered by the acid extraction process, but AlN is not acid-resistant. AlN can be found in inclusions similar to TiC subgrains rather than

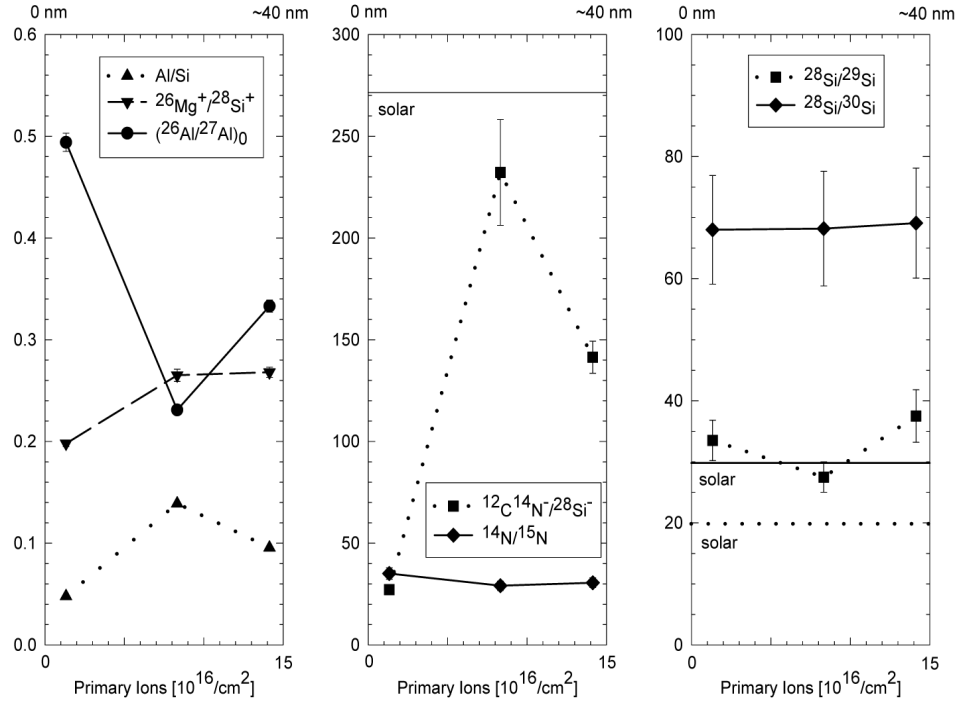

Fig. 3. Depth profiles for selected isotope and elemental ratios in SN grain 177-1. The x-axis shows the applied primary ion density, which corresponds to the achieved depth shown at the top axis and is the same for all diagrams. The first plot shows the Al/Si and $^{26}Mg^{+}/^{28}Si^{+}$ ratios together with the inferred, initial $^{26}Al/^{27}Al$ ratio. The second plot shows the nitrogen abundance (given as $^{12}C^{14}N^{-}/^{28}Si^{-}$) and isotope ratio and the last plot the silicon isotope ratios. The solar isotope ratios are indicated by horizontal lines.

being in solid solution (Stroud and Bernatowicz 2005; Hynes et al. 2006), allowing acids to dissolve it at least partly and possibly deposit meteorite material within the AlN, explaining the found correlation for the Tieschitz grains. For the Murchison grains, which do show a correlation between Li, Mg, and K, as well as between Al and Ca, contamination could have also been taken up by defects in the SiC crystal structure (holes, cracks), which would lead to positive correlations between trace elements Li, Mg, and K. Pits on surfaces of acid residue grains have been observed before (Bernatowicz et al. 2003) and attributed to etching of crystal defects on the surface of the grains.

The contamination by host material could also explain the higher elemental abundances for most elements for Tieschitz grains compared to the Murchison grains. The less harsh extraction process used for the Tieschitz grains might not have removed meteoritic material as well as for the Murchison grains. An exception is the Li abundance, which is higher for Murchison grains.

Grain alteration processes in the interstellar medium are expected to affect all SiC grains basically in the same way. Only if the SiC grains from Tieschitz and Murchison formed at different locations and/or times in our galaxy different alteration histories can be envisioned. The likelihood for this, however, is very low considering the formation history of the parent bodies of primitive meteorites, and this scenario can therefore be ruled out.

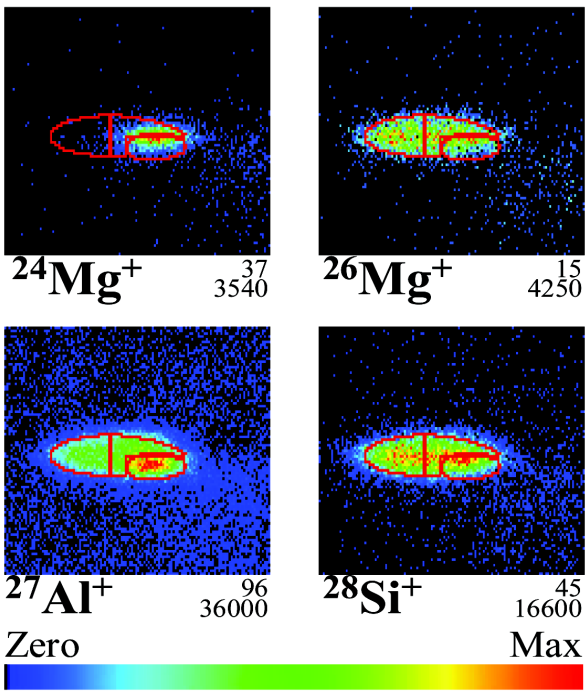

Fig. 4. Positive secondary ion images of ^{24}Mg, ^{26}Mg, ^{27}Al, and ^{28}Si in SN grain 480-3. The grain is divided into three distinct areas, named A, B, and C from left to right. The count rate for the most intense pixel and the number of total counts is indicated in the bottom right of the image. Field of view is 10 × 10 μm^2.

Table 5. Correlation coefficients for Murchison SiC grains. Bold numbers indicate a level of confidence above 99.8% whereas all others are well below 90%.

Murchison	Li	Mg	Al	K	Ca	Sc	Ti	V
Li	1							
Mg	**0.85**	1						
Al	0.03	0.35	1					
K	**0.97**	**0.88**	0.06	1				
Ca	–0.05	0.30	**0.96**	0.04	1			
Sc	–0.16	–0.07	0.15	–0.10	0.24	1		
Ti	–0.31	–0.38	–0.15	–0.29	–0.07	**0.90**	1	
V	–0.26	–0.34	–0.15	–0.28	–0.09	**0.87**	**0.96**	1

Table 6. Correlation coefficients for Tieschitz SiC grains. Bold numbers indicate a level of confidence above 97.5% whereas all others are below that limit, mostly below 90%.

Tieschitz	Li	Mg	Al	K	Ca	Sc	Ti	V
Li	1							
Mg	**0.57**	1						
Al	**0.81**	**0.69**	1					
K	**0.67**	**0.52**	**0.79**	1				
Ca	**0.52**	**0.49**	**0.71**	**0.63**	1			
Sc	–0.74	–0.72	–0.69	–0.77	–0.55	1		
Ti	–0.32	–0.18	–0.38	–0.36	–0.42	**0.90**	1	
V	–0.13	–0.23	–0.25	–0.51	–0.32	0.82	**0.89**	1

Huss and Lewis (1995) showed that part of the presolar grain population in the Tieschitz meteorite is destroyed when compared to abundances in unaltered meteorites. This destruction process could in principal also lead to alteration of grains. This would imply changes in the isotope ratios, especially for trace elements, toward solar system values. Differences in isotope ratios correlated with different host meteorites have not been reported yet despite analyses of thousands of grains from many different meteorites were performed. The only report of a shift in C isotope ratios toward ^{13}C-rich grains (Nittler and Alexander 2003) was explained by the difference in extraction methods. The use of a CsF technique appeared to lead to heavier C isotope ratios than the standard HF/HCl extraction method. Alteration in the host meteorite is therefore ruled out as source for the observed alterations.

The correlation between Sc, Ti, and V becomes very plausible if one considers them to be in TiC sub grains, which have been found in presolar SiC (Stroud and Bernatowicz 2005; Hynes et al. 2006) and graphite grains (e.g., Croat et al. 2005). Scandium as well as V fit into the TiC crystal structure and these elements should therefore be linked to the stellar source of the grains and are probably indigenous.

Depth Profiles for Type X SiC Grains 480-3 and 177-1

Grain 177-1 shows an increase in the Al and CN abundance with depth that may be caused by the acid extraction process. Although this grain experienced sputtering in the IMS3f before, part of the rim produced by the acid treatment might have survived. If AlN is dissolved in the rim of the grain as was reported before (Stephan and Jessberger 1997), then the ^{27}Al and ^{26}Mg might easily be affected differently and therefore the $(^{26}Al/^{27}Al)_0$ ratio changes. In contrast, the Si and N isotope ratios do not change with depth showing that most of this material must be of presolar origin and intrinsic to the grain, not being seriously affected by solar material sticking to it. Therefore, we conclude that the change in the $(^{26}Al/^{27}Al)_0$ ratio is not correlated to the condensation chemistry in the SN ejecta but is due to the extraction process.

The situation for grain 480-3 is different. Similar to grain 177-1, the Si and N isotope ratios clearly show a presolar origin, which means that only minor contributions from solar N- and Si-bearing matrix material might be sticking to the grain. Other than in grain 177-1, the ^{27}Al and ^{26}Mg abundances show relatively small changes with depth. Although grain 480-3 experienced the same extraction and measurement (ion imaging in the IMS3f) procedure as grain 177-1, the way the rim is affected must not be necessarily the same as this depends on factors such as, e.g., grain morphology and porosity. Thus we cannot exclude that, other than for grain 177-1, most of the rim of grain 480-3 was sputtered away before the TOF-SIMS measurements. Nevertheless, there are consistent heterogeneities found in the grain in the ^{27}Al abundance, which changes from the left side of the grain to the right side by nearly a factor of 3. Since ^{26}Mg, most of which is of radiogenic origin, is roughly constant across the grain, this implies changes in the inferred $(^{26}Al/^{27}Al)_0$ ratio that cannot be explained by the acid extraction process, which most likely would have shown changes with depth. There are two possibilities to explain our

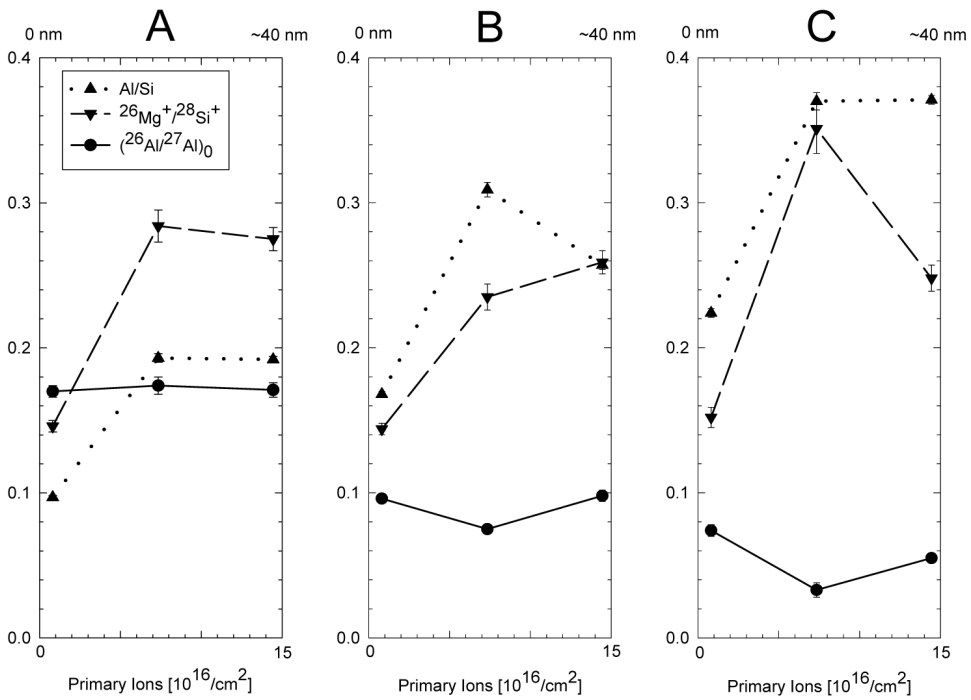

Fig. 5. Depth profiles for selected isotope and elemental ratios in SN grain 480-3 for three distinct regions.

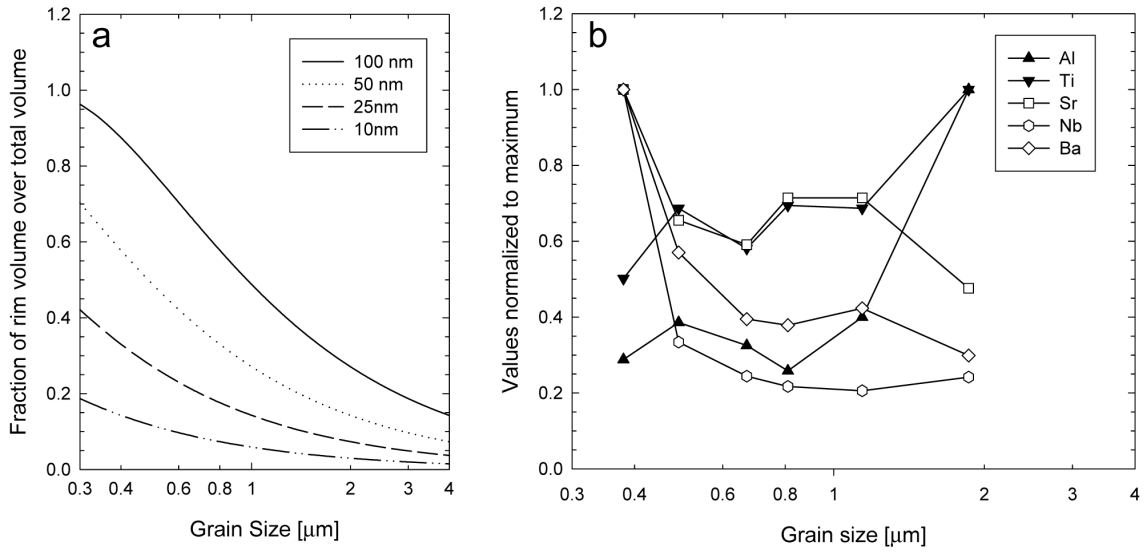

Fig. 6. The mass fraction of the particle within the rim, which could be affected by acid treatment, plotted against the particle size for different thicknesses of this rim in comparison with normalized elemental abundances from analyses of different grain sizes (Amari et al. 1995 and references therein).

finding: i) A local Al-rich contamination (thicker than the original rim) stuck to the grain surface, even after the DF-SIMS measurements and intense sputtering, or ii) the heterogeneity was established during grain formation in the SN ejecta, indicating temporal and/or spatial changes in the condensation conditions or changes in the SN gas composition.

There are different models how grains might condense in a supernova environment. The most common explanation is that material from different zones mixes to account for the observed isotope ratios. Simulations have shown the feasibility of such mixing (Burrows et al. 1995; Herant et al. 1994), before it was observed several years later (Irion 2000). The whole process, mixing in the supernova and grain formation following this mixing, has to occur within several months (Hoppe and Besmehn 2002), leaving only a very short

time for homogenization of the stellar gas source. To preserve the condition C/O > 1 for SiC condensation, the proposed scenarios of mixing different SN zones have been selective by considering matter from the inner Ni- and Si-rich zones along with material from the outer C-rich zones, but with only minor contributions from the intermediate O-rich zones (Travaglio et al. 1999; Hoppe et al. 2000). It is thus conceivable that isotope and elemental heterogeneities are preserved in the portion of the SN ejecta from which the SiC X grains condensed.

An alternative to the large-scale mixing scenario is condensation of SiC from matter from the inner Si-rich zones followed by modification on their way out through the overlying SN gas clouds due to several reverse shocks resulting in sputtering and implantation (Deneault et al. 2003). This model could explain a layered structure within the grains as long as they are not homogenized by other processes later on.

Both models might easily lead to isotopically and chemically heterogeneous grains. If the observed heterogeneity in grain 480-3 is not simply produced by contamination, then it may reflect the grain formation process. However, from the observed heterogeneity in the $(^{26}Al/^{27}Al)_0$ ratio and ^{27}Al abundances a clear conclusion on how the grain formed is not possible.

Implications

If the grains are indeed affected by the extraction process to a depth of several tens of nanometers, then this might have especially affected DF-SIMS measurements of small (submicrometer-sized) presolar SiC grains. Amari et al. (1995, 2000) reported variations in elemental and isotopic abundances for different size fractions of Murchison SiC grains. For these measurements, hundreds to thousands of grains were measured at once for better signal levels and therefore it is not possible to distinguish between material sputtered from outer layers or from the inner part of grains.

Figure 6 shows the fraction of the total volume an outer layer would have for a spherical volume against the grain size and the abundances of Al, Ti, Sr, Nb, and Ba versus the average grain size normalized to the maximum value within that range (data from Amari et al. 1995). Aluminum and Ti show an increase in abundance with grain size, whereas Sr, Nb, and Ba show a decrease with grain size. The model lines are calculated for 10, 25, 50, and 100 nm outer layer thicknesses. This simple model does not take into account the mechanism of deposition of any contamination or sputter mechanics. In general, there is always the possibility of leaching out material from the affected, outer layer, leading to an increase with depth, or meteoritic host material might be deposited in this outer layer, resulting in a decrease with depth. The trends in Fig. 6b do not show exactly the same curve as the model lines but the size variations for these minor elements in presolar grains might be an alteration of the presolar SiC grains during the extraction process. This means that trace element data from acid-residue grains should be treated carefully as they might be affected by the extraction technique. This is especially important for grains smaller than ~1 μm. It also brings up the need for measurements of unaltered presolar grains either in situ or extracted without the use of acids (Bernatowicz et al. 2003; Tizard et al. 2005).

The question on the origin of the observed heterogeneities in $^{26}Al/^{27}Al$ in the Tieschitz X-grain 480-3 cannot be unequivocally answered. Nevertheless, it adds to other observed isotopic heterogeneities within SN grains, such as the Si and Ca isotopic compositions in SiC X grains (Besmehn and Hoppe 2003) and the C and O isotopic compositions in graphite (Stadermann et al. 2005).

SUMMARY

Single presolar SiC grains were studied by analyzing element abundances and isotope ratios simultaneously by TOF-SIMS. The low sample consumption of only a few atomic layers made it possible to do several measurements without completely destroying the grains. Depth profiling was performed using a high-current, low-energy ion gun to sputter the particles at higher rates. Even grains, which have undergone several measurements, are still mainly intact for further studies.

The high lateral resolution made it possible to analyze elemental and isotopic heterogeneities within the micrometer-sized particles. In two out of three SN grains, we found heterogeneities with depth (grain 177-1) or lateral heterogeneities (grain 480-3) of Mg, Al, and the inferred initial $^{26}Al/^{27}Al$ ratio. The first can be explained by the chemical extraction process during which the host material is dissolved by acids and deposited within the grains. For the second grain, the heterogeneity does not show up in the depth profile, but as a lateral distribution that can either be explained by contamination with meteoritic material or by isotopic and elemental heterogeneities of the SN reservoir from which the grains condensed. The contamination of grains with meteoritic host material will alter isotopic and abundance data of trace elements, specifically when acquired for bulk samples consisting of submicrometer-sized grains. This shows the necessity of the use of acid-free sample preparation to minimize the contamination problem.

Acknowledgments–This work was supported by the Max-Planck-Institut für extraterrestrische Physik, Garching, Germany. We are grateful to Frank J. Stadermann, Scott Messenger, and Associate Editor Larry R. Nittler for their critical and helpful reviews.

Editorial Handling—Dr. Larry Nittler

REFERENCES

Amari S., Hoppe P., Zinner E., and Lewis R. S. 1992. Interstellar SiC with unusual isotopic compositions: Grains from a supernova? *The Astrophysical Journal* 394:L43–L46.

Amari S., Hoppe P., Zinner E., and Lewis R. S. 1995. Trace-element concentrations in single circumstellar silicon carbide grains from the Murchison meteorite. *Meteoritics* 30:679–693.

Amari S., Lewis R. S., and Anders E. 1994. Interstellar grains in meteorites: I. Isolation of SiC, graphite, and diamond; size distributions of SiC and graphite. *Geochimica et Cosmochimica Acta* 58:459–470.

Amari S., Zinner E., and Lewis R. S. 2000. Isotopic compositions of different presolar silicon carbide size fractions from the Murchison meteorite. *Meteoritics & Planetary Science* 35:997–1014.

Anders E. and Zinner E. 1993. Interstellar grains in primitive meteorites: Diamond, silicon carbide, and graphite. *Meteoritics* 28:490–514.

Bernatowicz T., Fraundorf G., Tang M., Anders E., Wopenka B., Zinner E., and Fraundorf P. 1987. Evidence for interstellar SiC in the Murray carbonaceous meteorite. *Nature* 330:728–730.

Bernatowicz T. J., Messenger S., Pravdivtseva O., Swan P., and Walker R. M. 2003. Pristine presolar silicon carbide. *Geochimica et Cosmochimica Acta* 67:4679–4691.

Burrows A., Hayes J., and Fryxell B. A. 1995. On the nature of core-collapse supernova explosions. *The Astrophysical Journal* 450: 830–850.

Besmehn A. and Hoppe P. 2003. A NanoSIMS study of Si- and Ca-Ti-isotopic compositions of presolar silicon carbide grains from supernovae. *Geochimica et Cosmochimica Acta* 67:4693–4703.

Croat T. K., Stadermann F. J., and Bernatowicz T. J. 2005. Presolar graphite from AGB stars: Microstructure and *s*-process enrichment. *The Astrophysical Journal* 63:976–987.

Deneault E. A. N., Clayton D. D., and Heger A. 2003. Supernova reverse shocks: SiC growth and isotopic composition. *The Astrophysical Journal* 594:312–325.

Floss C., Stadermann F. J., Bradley J. P., Dai Z. R., Bajt S., Graham G., and Lea A. S. 2006. Identification of isotopically primitive interplanetary dust particles: A NanoSIMS isotopic imaging study. *Geochimica et Cosmochimica Acta* 70:2371–2399.

Henkel T., Stephan T., Jessberger E. K., Hoppe P., and Strebel R. 2000. Structured presolar silicon carbide X grains (abstract)? *Meteoritics & Planetary Science* 35:A69–A70.

Henkel T., Stephan T., Jessberger E. K., Hoppe P., Strebel R., Amari S., Zinner E. K., and Lewis R. S. 2002. TOF-SIMS analysis of 13 presolar silicon carbide grains (abstract). *Meteoritics & Planetary Science* 37:A61.

Herant M., Benz W., Hix W. R., Fryer C. L., and Colgate S. A. 1994. Inside the supernova—A powerful convective engine. *The Astrophysical Journal* 435:339–361.

Hoppe P. and Besmehn A. 2002. Evidence for extinct vanadium-49 in presolar silicon carbide grains from supernovae. *The Astrophysical Journal* 576:L69–L72.

Hoppe P. and Zinner E. 2000. Presolar dust grains from meteorites and their stellar sources. *Journal of Geophysical Research* 105: A10,371–A10,385.

Hoppe P., Strebel R., Eberhardt P., Amari S., and Lewis R. S. 2000. Isotopic properties of silicon carbide X grains from the Murchison meteorite in the size range 0.5–1.5 μm. *Meteoritics & Planetary Science* 35:1157–1176.

Huss G. R. and Lewis R. S. 1995. Presolar diamond, SiC, and graphite in primitive chondrites: Abundances as a function of meteorite class and petrologic type. *Geochimica et Cosmochimica Acta* 59: 115–160.

Hynes K. M., Croat T. K., Amari S., Mertz T. F., and Bernatowicz T. 2006. A transmission electron microscopy study of ultramicrotomed SiC-X grains (abstract #2202). 37th Lunar and Planetary Science Conference. CD-ROM.

Irion R. 2000. Astrophysics—Supernova pumps iron in inside-out blast. *Science* 287:203–205.

Jochum K. P., Dingwell D. B., Rocholl A., Stoll B., Hofmann A. W., Becker S., Besmehn A., Bessette D., Dietze H. J., Dulski P., Erzinger J., Hellebrand E., Hoppe P., Horn I., Janssens K., Jenner G. A., Klein M., McDonough W. F., Maetz M., Mezger K., Münker C., Nikogosian I. K., Pickhardt C., Raczek I., Rhede D., Seufert H. M., Simakin S. G., Sobolev A. V., Spettel B., Straub S., Vincze L., Wallianos A., Weckwerth G., Weyer S., Wolf D., and Zimmer M. 2000. The preparation and preliminary characterisation of eight geological MPI-DING reference glasses for in situ microanalysis. *Geostandards Newsletter* 24:87–133.

Kashiv Y., Cai Z., Lai B., Sutton S. R., Lewis R. S., Davis A. M., Clayton R. N., and Pellin M. J. 2001. Synchrotron X-ray fluorescence: A new approach for determining trace element concentrations in individual presolar SiC grains (abstract #2192). 32nd Lunar and Planetary Science Conference. CD-ROM.

Kashiv Y., Cai Z., Lai B., Sutton S., Lewis R. S., Davis A. M., Clayton R. N., and Pellin M. J. 2002. Condensation of trace elements into presolar SiC stardust grains (abstract #2056). 33rd Lunar and Planetary Science Conference. CD-ROM.

Lewis R. S., Tang M., Wacker J. F., Anders E., and Steel E. 1987. Interstellar diamonds in meteorites. *Nature* 326:160–162.

Lodders K. and Amari S. 2005. Presolar grains from meteorites: Remnants from the early times of the solar system. *Chemie der Erde* 65:93–166.

Mostefaoui S. and Hoppe P. 2004. Discovery of abundant in situ silicate and spinel grains from red giant stars in a primitive meteorite. *The Astrophysical Journal* 613:L149–L152.

Nguyen A. N. and Zinner E. 2004. Discovery of ancient silicate stardust in a meteorite. *Science* 303:1496–1499.

Nittler L. R. 2003. Presolar stardust in meteorites: Recent advances and scientific frontiers. *Earth and Planetary Science Letters* 209: 259–273.

Nittler L. R. and Alexander C. M. O'D. 2003. Automated isotopic measurements of micron-sized dust: Application to meteoritic presolar silicon carbide. *Geochimica et Cosmochimica Acta* 67: 4961–4980.

Rost D., Stephan T., and Jessberger E. K. 1999. Surface analysis of stratospheric dust particles. *Meteoritics & Planetary Science* 34: 637–646.

Stadermann F. J., Croat T. K., Bernatowicz T. J., Amari S., Messenger S., Walker R. M., and Zinner E. 2005. Supernova graphite in the NanoSIMS: Carbon, oxygen, and titanium isotopic compositions of a spherule and its TiC sub-components. *Geochimica et Cosmochimica Acta* 69:177–188.

Stephan T. 2001. TOF-SIMS in cosmochemistry. *Planetary and Space Science* 49:859–906.

Stephan T. and Jessberger E. K. 1996. TOF-SIMS analysis of interstellar SiC grains (abstract). 27th Lunar and Planetary Science Conference. pp. 1267–1268.

Stephan T., Rost D., Jessberger E. K., Budell R., Greshake A., Zinner E. K., Amari S., Hoppe P., and Lewis R. S. 1997. TOF-SIMS analysis of SiC grains with high lateral resolution (abstract). 28th Lunar and Planetary Science Conference. pp. 1371–1372.

Strebel R. 1998. SIMS studies of presolar silicon carbide and Al-rich oxide grains from acid-resistant meteorite separates. Ph.D. thesis, Universität Bern, Switzerland.

Stroud R. M. and Bernatowicz T. 2005. Surface and internal structure

of pristine presolar silicon carbide. (abstract #2010) 36th Lunar and Planetary Science Conference. CD-ROM.

Tizard J., Henkel T., and Lyon I. 2005. The gentle separation of presolar SiC grains from meteorites. *Meteoritics & Planetary Science* 40:335–342.

Travaglio C., Gallino R., Amari S., Zinner E., Woosley S., and Lewis R. S. 1999. Low-density graphite grains and mixing in type II supernovae. *The Astrophysical Journal* 510:325–354.

Zinner E. K. 2004. Presolar grains. In *Meteorites, comets, and planets*, edited by Davis A. M. Treatise on Geochemistry, vol. 1. Oxford and San Diego: Elsevier. pp.17–39.